Adsorption (2015) 21:419–432
DOI 10.1007/s10450-015-9683-7

Adsorption kinetics of CO_2, CO, N_2 and CH_4 on zeolite LiX pellet and activated carbon granule

Youngsan Ju[1] · Yongha Park[1] · Dooyoung Park[1] · Jae-Jeong Kim[1] · Chang-Ha Lee[1]

Received: 3 April 2015 / Revised: 22 June 2015 / Accepted: 23 June 2015 / Published online: 30 June 2015

Abstract The adsorption uptake curves of CO_2, CO, N_2 and CH_4 on zeolite LiX and activated carbon were measured using a volumetric method at 293, 308 and 323 K and pressure up to 100 kPa. The experimental uptake curves were correlated with a non-isothermal kinetic model because the adsorption kinetics was controlled by heat generation and transfer, and an isothermal model showed large deviation from experimental uptake. The adsorption rates of the gases on zeolite LiX and activated carbon were affected by the isosteric heat of adsorption, heat transfer rate and adsorption affinity. At the same pressure and temperature, the sequence of effective diffusion time constants was $CO_2 \ll CO < N_2 < CH_4$ for zeolite LiX and $CO_2 \ll CH_4 \le N_2 < CO$ for activated carbon. The adsorption rate of CO showed the largest difference between the two adsorbents. Effective diffusion time constants (D/R^2) for all cases were provided, which depended on pressure and temperature.

Keywords Activated carbon · Zeolite LiX · Adsorption kinetics · Heat of adsorption · Non-isothermal model

List of symbols

a	External surface area divided by the volume of the adsorbent (m^{-1})
c_p	Concentration in the particle (mol kg^{-1})
C_s	Heat capacity of the sample (J g^{-1} K^{-1})
D/R^2	Effective diffusion time constant (s^{-1})
D	Diffusivity (m^2 s^{-1})
D_c/r_c	Micropore diffusion time constant (s^{-1})
D_p/R_p	Effective macropore diffusion time constant (s^{-1})
h	Overall heat transfer coefficient (J m^{-1} s^{-1} K^{-1})
K	Henry constant (–)
P	Pressure (kPa)
Q	Adsorbed amount (mol kg^{-1})
Q_{st}	Isosteric heat of adsorption (kJ mol^{-1})
R	Ideal gas constant (J mol^{-1} K^{-1})
R^2	Coefficient of determination (R^2) (–)
T	Time (s)
T	Temperature (K)
V_g	Volume occupied by the gas (m^3)
V_s	Volume occupied by the adsorbent (m^3)
α	Dimensionless parameter defined by non-isothermal model (–)
β	Dimensionless parameter defined by non-isothermal model (–)
ρ_s	Density of the adsorbent (g m^{-3})

Subscript

0	Initial state
∞	Equilibrium state

1 Introduction

Recently, the reduction of greenhouse gas (GHG) emissions has been emphasized in various industrial fields in order to prevent global warming. Therefore, many adsorptive technologies have been reported to recover clean fuel sources (H_2, CH_4, CO, etc.) and to capture CO_2 from various effluent gases.

Since H_2, CH_4 and CO are used as chemical raw materials or as clean fuel sources, great needs from various industrial fields lead to strong economic motivation for the development of adsorption processes to recover these gases

✉ Chang-Ha Lee
leech@yonsei.ac.kr

[1] Department of Chemical and Biomolecular Engineering, Yonsei University, Seoul, Korea

from reforming gas, syngas, coke oven gas, bio-gas and more traditional sources (Lee et al. 2008; Grande and Rodrigues 2007; Ahn et al. 2001; Yang and Lee 1998). For example, efficient H_2 recovery from the off-gas of the integrated gasification combined cycle (IGCC) is an important issue for green power generation (Lee et al. 2014b). After carbon capture in the IGCC, recovered H_2 can be used to power hydrogen turbines and as a renewable energy source.

Pressure or vacuum swing adsorption (PSA or VSA) process using porous adsorbents is a promising process for such purpose which can meet the requirement for high separation efficiencies with respect to energy and environmental targets. To select proper adsorbents and to design efficient adsorption processes, adsorption equilibrium and kinetic data for each component on a porous adsorbent are the most important factors. The effluent gases from traditional and non-traditional processes consist of 3–6 major components after various pretreatment processes including particle removal, drying and/or large molecule removal. For example, the coal gasifier in the IGCC generates a mixture gas containing CO_2, CO, N_2, CH_4, Ar and H_2 (Lee et al. 2014a). Bio-gas and natural gas are mainly composed of CH_4, CO_2 and N_2 (Cavenati et al. 2006; Grande and Rodrigues 2007). Coke oven gas and other effluent gases from iron and steel industries contain H_2, CH_4, CO_2, N_2, and CO, and reforming gas in petrochemical industries consists of H_2, CO_2, CH_4 and CO as a main component (Yang and Lee 1998; Ahn et al. 2001). In many studies of adsorption processes, two different adsorbents such as activated carbons and zeolites are simultaneously applied to one adsorptive unit for optimal process design (You et al. 2012; Ahn et al. 2001, 2012; Cavenati et al. 2006; Siriwardane et al. 2001). Naturally, to meet the proper selection criteria for designing the processes, the kinetic behaviors and thermodynamic characteristics of various gases in adsorbents should be understood.

In adsorptive processes, pelletized adsorbents are generally packed into an adsorption bed to minimize pressure drop in the bed. Zeolite pellets consist of micropores in zeolite crystal, macropores among zeolite crystals and binder. Therefore, studies have analyzed the contributions of macropores and micropores in the rate-determining step of N_2, CH_4 and CO_2 in zeolite 4A, 5A, CaX and 13X pellets (Ahn et al. 2002, 2004; Silva et al. 2012; Hu et al. 2014). In a carbon molecular sieve, controlled micropores significantly affect the adsorption kinetics, and the kinetic difference among adsorbates strongly depends on molecular size and adsorption affinity (Bae and Lee 2005; Giesy and LeVan 2013; Yang et al. 2014). There are few studies of adsorption kinetics of activated carbon granules with wide pore size distribution from micropores to macropores (Gray and Do 1991; Himeno et al. 2005).

In this study, the adsorption kinetics of four pure components (CO_2, CO, N_2 and CH_4) on commercial activated carbon granules and zeolite LiX pellets is described because these components are generally found in H_2 off-gases and various effluent gases. The adsorption of H_2 and Ar was too fast to evaluate their adsorption rates on the adsorbents. The adsorption uptake curves were measured using a volumetric method at three different temperatures of 293, 308 and 323 K and pressures up to 100 kPa. The effective diffusion time constants (D/R^2) of each component on each adsorbent at various pressure and temperature conditions were obtained by correlating a non-isothermal kinetic model with experimental uptake curves. The effect of adsorption heat on adsorption kinetics was evaluated by comparing the results of isothermal and non-isothermal kinetic models. The controlling mechanism of diffusion in zeolite LiX was determined by comparison of the effective diffusion time constants of different sizes of zeolite pellets. The results allow optimized design of various adsorptive processes for H_2 recovery and CO_2 capture.

2 Theory

In a volumetric system, a certain amount of adsorbate gas is injected into the cell, and the pressure is monitored until it reaches an equilibrium state. The pressure change was calculated based on the amount adsorbed using the virial coefficients and known volume of the adsorption cell.

The adsorbents, activated carbon and/or zeolite, packed in the adsorption bed have a certain range of granule or pellet size. In the study, a certain number of adsorbents were used in the adsorption cell as received from manufacturers. Since both micropore and macropore diffusions are described by the same form of Fick's diffusion law, the effective diffusion time constant could be interpreted as a micropore diffusivity (D_c/r_c^2) or effective macropore diffusivity (D_p/R_p^2), depending on the controlling diffusion mechanism of each system. In the study, the effective diffusion time constant (D/R^2) obtained from the experimental uptake curve was assumed to reflect the overall diffusion mechanism of an adsorbate in various pores of the adsorbent pellet.

The adsorption kinetic model for experimental uptake is derived from Fick's diffusion law in the cell assuming constant diffusivity (D). To analyze the adsorption kinetics, the simplest analytical solution for a constant volume system, which assumes isothermal condition and a linear equilibrium relationship, was derived as follows: (Crank 1956)

$$\frac{M_\infty - M_t}{M_\infty - M_0} = \sum_{n=1}^{\infty} \frac{6\alpha'(\alpha'+1)}{9\alpha'+9+\alpha'^2\beta_n^2} \exp\left(-\beta_n^2 \frac{D}{R^2} t\right) \quad (1)$$

where

$$\tan\beta_n = \frac{3\beta_n}{3+\alpha'\beta_n^2} \quad (2)$$

$$\alpha' = \frac{3V}{4\pi R^3 K} \quad (3)$$

In Eqs. (1)–(3), M_t, M_0 and M_∞ represent the amount adsorbed at ambient time t, initial time 0 and equilibrium, respectively, V is the volume of the system, R is the radius of the adsorbent sample and K is the effective Henry's law constant at a corresponding pressure interval in a stepwise change.

When the isothermal model is applied to experimental data, a key factor that generates significant error is the heat effect generated by the heat of adsorption. The heat generated leads to increased temperature in the system, and heat is dissipated into the surroundings. Therefore, the adsorbate molecules diffuse faster at higher temperatures while adsorption of molecules on the adsorbent surface is retarded due to thermal resistance and equilibrium shift (Ahn et al. 2002, 2004; Do 1998). Due to the heat of adsorption, the former isothermal model was modified to reflect the non-isothermal condition induced by heat release (Kočiřík et al. 1984). The following equations are the analytical solution for a non-isothermal condition in a volumetric system:

$$\frac{M_\infty - M_t}{M_\infty - M_0} = \sum_{n=1}^{\infty} \frac{9\left(1+K\frac{V_s}{V_g}\right)\left[\frac{Y_n}{\beta_n^2}\right]^2 \exp\left(-\beta_n^2 \frac{D}{R^2} t\right)}{\frac{1}{\varphi_n} + \frac{3}{2}\frac{\beta'}{\varphi_n}\left[\beta_n \cot\beta_n \left(\frac{Y_n}{\beta_n^2}\right) + 1\right] + \frac{3}{2}K\frac{V_s}{V_g}\frac{1}{\beta_n^4}\frac{A_n}{\varphi_n}} \quad (4)$$

in which β_n are the roots of:

$$(-\beta_n + \alpha) + 3\beta Y_n - 3K\frac{V_s}{V_g}\frac{1}{\beta_n^2}(-\beta_n + \alpha)Y_n = 0 \quad (5)$$

and where

$$A_n = Y_n\left[\left(\beta_n^2 - \alpha\right)\beta_n \cot\beta_n - 2\alpha\right] + \beta_n^2\left(\beta_n^2 - \alpha\right) \quad (6)$$

$$Y_n = \beta_n \cot\beta_n - 1 \quad (7)$$

$$\frac{1}{\varphi_n} = \frac{1}{\beta}\left(1 - 3K\frac{V_s}{V_g}\frac{Y_n}{\beta_n^2}\right) \quad (8)$$

In Eqs. (4)–(8), V_s and V_g are the volume occupied by the solid and the gas, respectively.

In this model, two parameters (α, β) regarding the rate of heat transfer and heat of adsorption are defined as follows:

$$\alpha = \left(\frac{ha}{\rho_s C_s}\right) / \left(\frac{D}{R^2}\right) \quad (9)$$

$$\beta = \frac{\Delta H}{\rho_s C_s}\left(\frac{\partial q^*}{\partial T}\right)_{c_0, T_0} \quad (10)$$

where α is the external surface area divided by the volume of the adsorbent; ρ_s and C_s represent the density and heat capacity of the sample, respectively; h is the overall heat transfer coefficient; and ΔH is the heat of adsorption.

Parameter α describes the relative ratio of heat transfer ($ha/\rho_s C_s$) to effective diffusion time constant (D/R^2). Therefore, a large value of α implies that the heat generated during adsorption transferred into the surroundings rather than increasing the temperature of the adsorbent. A small value of α, on the other hand, implies that heat generation is concentrated at the initial part of the uptake because of the rapid uptake of molecules. Therefore, temperature increases during the adsorption, which reduces the equilibrium capacity. The slope of the uptake curve changes with time until heat is fully dissipated into the atmosphere.

Parameter β represents the heat of adsorption ($\Delta H/\rho_s C_s$) and the temperature dependence of the equilibrium capacity on the adsorbent ($\partial q^*/\partial T$). When the equilibrium shift with temperature increase is minor, the kinetic result is close to that predicted by the isothermal model. On the contrary, if an adsorbate has strong temperature dependence with a large value of β, the uptake curve deviates from the isothermal model, resulting in a heat transfer-controlled system.

The reliability of simultaneous non-linear regression for three parameters (α, β and D/R^2) in Eq. (4) is not guaranteed in general. Therefore, to obtain ($ha/\rho_s C_s$) and β as a first step, the kinetic model of an entirely heat-controlled system was presented in the asymptotic form of kinetic models as follows: (Hu et al. 2014; Lee and Ruthven 1979; Ruthven et al. 1980)

$$\frac{M_\infty - M_t}{M_\infty - M_0} = \frac{\beta}{1+\beta}\exp\left[\frac{-hat}{\rho_s C_s(1+\beta)}\right] \quad (11)$$

In the corresponding system, the uptake curve is linear on a semi-log scale for time t.

As a result, α and β were obtained first from the latter part of the experimental uptake curve by using Eq. (11), and then the effective diffusion time constant was obtained by fitting the entire uptake curve using the non-isothermal kinetic model, Eq. (4). In this approach, the secant method, incremental search method (ISM) and least-squares method were used for non-linear regression using MATLAB (Mathworks, Inc.). In addition, a few sets of uptake data were fitted using the isothermal model in order to evaluate the thermal effects on adsorption.

In this study, experimental deviation from the model was estimated by the following coefficient of determination (R^2):

$$R^2 = 1 - \frac{\sum (q_{exp} - q_{ni})^2}{\sum (q_{exp} - \bar{q})^2} \quad (12)$$

where q_{exp} was the experimental point; q_{ni} was the value from the non-isothermal kinetic model; and $\bar{q}$ was the mean value of the experimental data. When the model agreed well with the data, the value of R^2 approached 1.

3 Experimental section

3.1 Material

Spherical zeolite LiX pellets and cylindrical activated carbon granules were supplied by ZEOCHEM Co. (Z10-05-03) and KURARAY CHEMICAL Co. (coal-derived activated carbon; 2GA-H2J), respectively. The zeolite LiX and activated carbon were analyzed using an automatic volumetric sorption analyzer (BELSORP-Max) with CO_2 at 298 K. Table 1 presents the measured and supplied physical properties of the adsorbents. Gases used as adsorbates (CO_2, CO, N_2 and CH_4) were of high purity (>99.99 %).

3.2 Experimental procedure

A high-pressure volumetric system in Fig. 1 (BELSORP-HP) was used to measure adsorption equilibrium and uptake. Prior to the experimental run, zeolite LiX was regenerated at 623 K in an oven and activated carbon at 393 K in a vacuum oven for longer than 8 h. The mass of adsorbent was measured by a microbalance with an accuracy of ±10 μg.

Before deciding on the sample mass in the volumetric system, two sample masses (0.3922 and 0.8779 g) were tested for the N_2/zeolite LiX system at 293 K in a pressure range of 0–100 kPa. The difference between the uptake curves obtained from two different sample masses was very small and the effective diffusion time constants were almost the same within the experimental error range. However, a smaller amount of sample showed slightly more fluctuation in the isotherm measurement. In the study, 0.8779 g of zeolite LiX with the average pellet size of 1.5 mm and 1.3811 g of activated carbon were used for the experiments.

The adsorbent was placed into the adsorption cell with a ceramic cap (Swagelok SS-8-VCR-2-GR-.5M) with 0.5 μm pores after two He purge. Then, it was assumed that the flow resistance into the adsorption cell is negligible. To minimize error caused by moisture and any trace of pollutants adsorbed during the installation of the adsorption cell, the zeolite LiX and activated carbon in the cell were reactivated at 623 and 393 K, respectively, under vacuum for longer than 12 h.

The system, composed of gas storage tanks, lines, valves and gauges, was set in an air bath, while the temperature of the adsorption cell was controlled by a water bath circulator. Two temperature controllers for each air bath and water bath were used in order to keep the temperature of the internal system and adsorption cell constant. The internal volume of the system and the dead volume in the adsorption system were measured by using helium gas at an experimental temperature.

The internal system was purged with helium gas before experiments, followed by an evacuation process with vacuum pumps. After repeating the purge/vacuum step three times, a specified amount of adsorptive gas was released into the internal system. The experiment was carried out by injecting a small amount of adsorbate into the adsorption cell at a constant temperature, and the pressure variation was monitored with an electrical pressure sensor (Full scale: 0.133 MPa (abs) × 1 unit, Accuracy: ±0.08 % of full scale). Once equilibrium was reached, a certain amount of adsorbate was again injected into the adsorption cell, and this procedure was repeated with a stepwise pressure change. For each experiment, all thermodynamic and uptake data were recorded automatically on an interfaced computer. The amount of gas adsorbed was calculated from the measured data on temperature, volume and pressure based on the compressibility factors from NIST thermodynamic isotherm properties (Linstrom and Mallard 2001). The recorded pressure change was converted into fractional uptake data at the equilibrium pressure.

Table 1 Physical properties of adsorbents

Property	Zeolite LiX	Activated carbon
Type	Pellet	Cylindrical
Particle size (mm)	1.5–1.7	1.7–2.36
Particle porosity	0.64	0.43
BET surface area (m^2/g)	755	800
Pore volume (cm^3/g)	0.326	0.205
Pellet density (g/cm^3)	2.4	0.85
Heat capacity (J/g K)	1.76	1.05

4 Results and discussion

4.1 Comparison of isothermal and non-isothermal kinetic models

Five to six sets of uptake data for CO_2, CO, N_2 and CH_4 on zeolite LiX and activated carbon at 298, 308 and 323 K

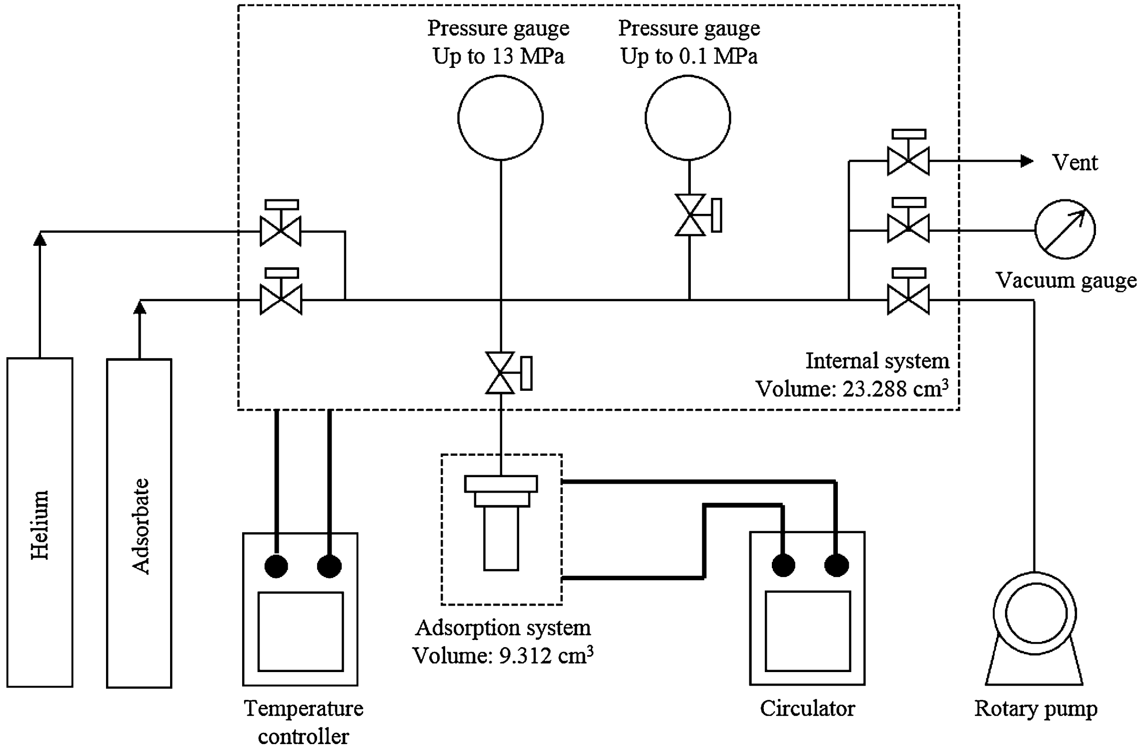

Fig. 1 Schematic diagram of volumetric apparatus

were compiled at similar pressure conditions for each adsorbate over a pressure range of 15–90 kPa. Since the kinetic models assume a linear equilibrium relationship, it was assumed for the linear relationship between pressures of a stepwise change in the range of 3–9 kPa, depending on the adsorbate and the pressure condition. The effective diffusion time constant was obtained by fitting each experimental uptake curve using a non-isothermal kinetic model.

Figures 2 and 3 represent the experimental uptake curves for CO_2, CO, N_2 and CH_4 at 293 K in zeolite LiX and activated carbon, respectively. The non-isothermal kinetic model predicted reasonably well the experimental uptake curve for each adsorbate with R^2 values higher than 0.98 for all gases. As a representative case, the isothermal model results for CH_4 on zeolite LiX and CO on activated carbon are shown in Figs. 2 and 3. The same effective diffusion time constant obtained from the non-isothermal model was applied to the isothermal model.

Over the range of measurement time, the isothermal model predicted the uptake curves during the initial period time, but the deviation from the experimental results increased with time even though their heats of adsorption were smaller than that of CO_2, as shown in Fig. 4. The adsorption of the adsorbates on zeolite LiX and activated carbon was disturbed by a thermal effect and was completely controlled by the heat when approaching

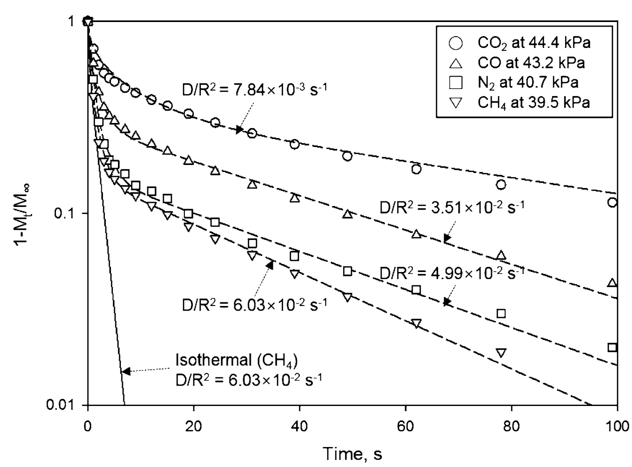

Fig. 2 Experimental and theoretical uptake curves of various gases on zeolite LiX at 293 K: *short dashed line* non-isothermal diffusion model; *solid line* isothermal diffusion model

equilibrium. The result implied that isothermal diffusion at the initial period time was changed to the non-isothermal diffusion by the heat release from the heat of adsorption with time. Although the non-isothermal model accurately predicted the experimental uptake curves, the deviation from the CO_2 uptake curve was relatively higher than that of the other curves. The assumptions of constant diffusivity and instantaneous equilibration of adsorbate in the

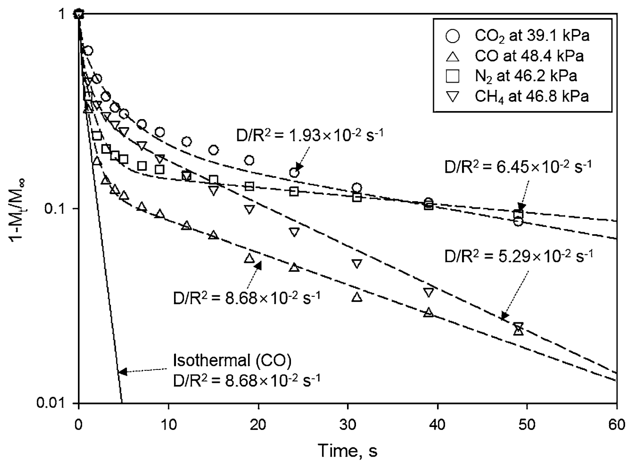

Fig. 3 Experimental and theoretical uptake curves of various gases on activated carbon at 293 K: *short dashed line* non-isothermal diffusion model; *solid line* isothermal diffusion model

experimental range might lead to greater deviation in the CO_2 uptake curve than in those of the other components.

4.2 Adsorptive kinetic behaviors

The isosteric heat of adsorption and the adsorption isotherm are key factors that affect adsorption rate. Because the high isosteric heat of adsorption arises from a strong affinity, it increases the molecular diffusion rate but prevents adsorption on the adsorbent surface. In general, a slower adsorption rate is expected at a higher isosteric heat of adsorption. To explain the adsorptive kinetic behaviors, the adsorption isotherms and the isosteric heats of adsorption for all gases on zeolite LiX and activated carbon are presented in the same experimental pressure range in Figs. 4a and b, respectively.

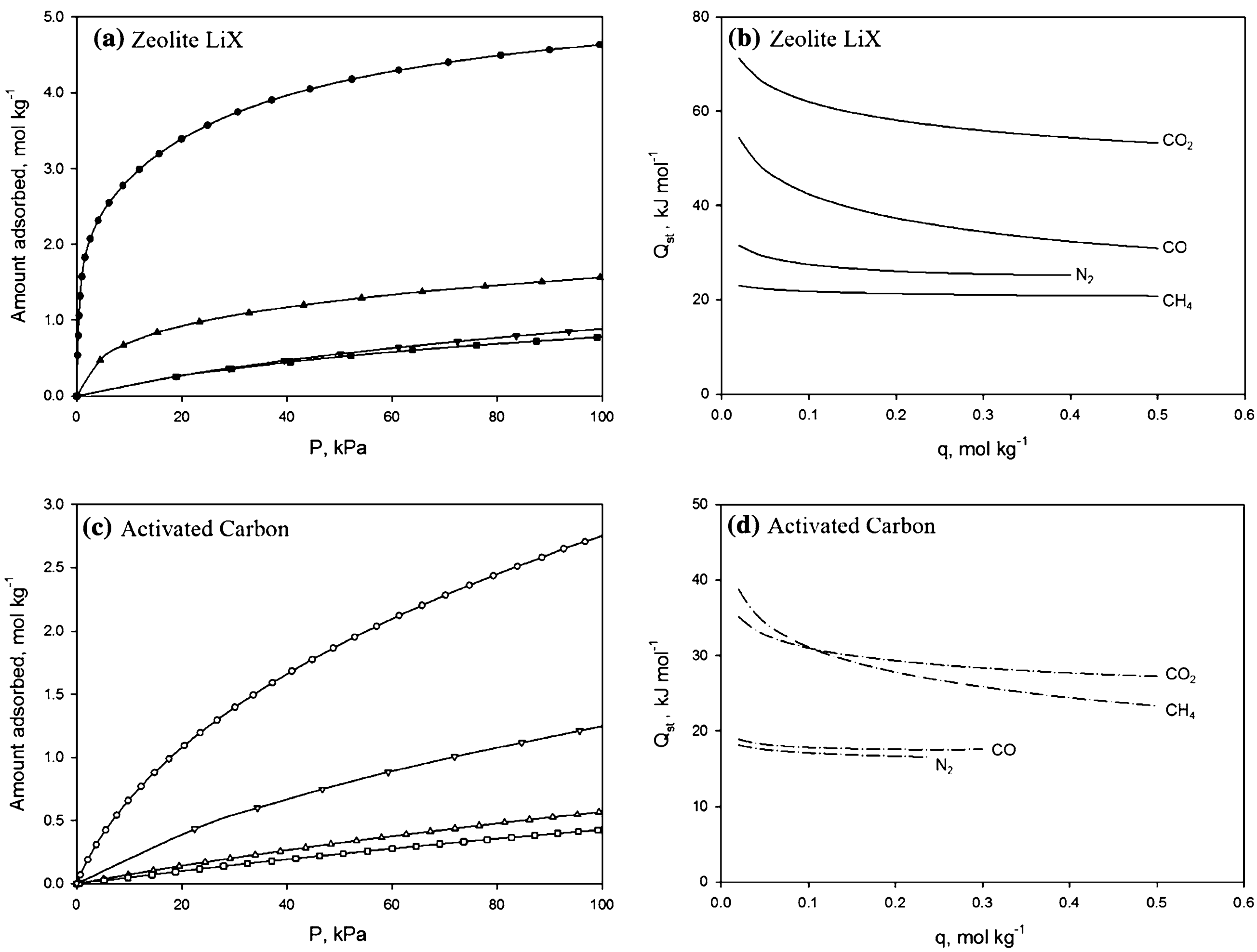

Fig. 4 Adsorption isotherms at 293 K and isosteric heats of adsorption on adsorbents with respect to the adsorbed amount on **a**, **b** zeolite LiX and **c**, **d** activated carbon: (*circle* CO_2; *up-pointing triangle* CO; *square* N_2; *down-pointing triangle* CH_4) (Data from Park et al. 2014)

As shown in Fig. 4, the adsorption isotherm and heat of adsorption of N_2 on activated carbon were the lowest in all the adsorbate/adsorbent systems. In Figs. 2 and 3, the uptake curve of N_2 on activated carbon was curved around 5–7 s more steeply than the other curves. This uptake curve indicates that the adsorption of N_2 occurred mainly in the initial time period, but the adsorption rate of N_2 with relatively weak adsorption affinity was affected by a thermal effect even though the heat of adsorption was relatively low. However, the result could be expected for fast thermal equilibrium in the N_2/activated carbon system.

The effective diffusion time constants obtained from the uptake curves are listed in Tables 2 and 3, and presented in Fig. 5. The order of adsorption rate on zeolite LiX was $CO_2 \ll CO < N_2 < CH_4$ at 293 K over the whole pressure range, as shown in Fig. 5a. In Fig. 4b, the isosteric heats of adsorption of CO_2, CO, N_2 and CH_4 on zeolite LiX were $CH_4 < N_2 < CO \ll CO_2$, which is opposite the adsorption rate order. For adsorption on activated carbon, the order of adsorption rate was $CO_2 \ll CH_4 \leq N_2 < CO$. According to Fig. 4b, the sequence of adsorption rates of gases was not perfectly matched with the order of the isosteric heat of adsorption: $N_2 \leq CO < CH_4 < CO_2$.

Because the heat generation is concentrated at the early stage, the influence of heat of adsorption on adsorption rate is quite strong at this stage. On the other hand, when the system approaches equilibrium, the adsorption rate is more affected by heat transfer rather than heat generation. The contributions of these two effects to the adsorption rate differ among adsorbate/adsorbent systems.

As mentioned in the non-isothermal kinetic model in Eq. (4), the effective diffusion time constant was affected by the two parameters of heat of adsorption (β) and rate of heat transfer (α). The values used for the non-isothermal kinetic model are listed in Tables 2 and 3. The relative heat transfer rates of gases, α, represents the influence of the heat transfer rate ($ha/\rho_s C_s$) compared to the diffusion rate. Therefore, if the system has a large α value, it is controlled by adsorption affinity due to immediate heat release. In the opposite case, the contribution of slow heat transfer to adsorption rate is increased because the generated heat precludes additional adsorption on the surface.

The adsorption rate of CO_2 with the largest isosteric heat of adsorption on activated carbon was slower than that of the other gases. However, the adsorption rate of N_2, which was expected to be the fastest, was similar to that of CH_4. When comparing approximate heat transfer rates in terms of α, CO_2 and CH_4 were greater than 1, whereas N_2 and CO were 0.24 and 0.50 respectively. Therefore, due to relatively slow heat transfer, the adsorption of N_2 on the activated carbon surface is disturbed by the generated heat. Consequently, the adsorption uptake curve for activated carbon is drastically changed, as shown in Fig. 3. In addition, Fig. 4a implies that N_2 and CO had low adsorption affinity on activated carbon, resulting in low isosteric heats of adsorption. As a result, a slower than expected adsorption rate for N_2 and CO was observed on activated carbon.

In the case of zeolite LiX, CO_2 had an α of 1.8, while the others (CO, N_2 and CH_4) had values of 0.81, 0.58 and 0.56, respectively. Although the relative heat transfer rate for CO_2 was faster than those of the others, the approximately 2–3 times higher isosteric heat of adsorption shown in Fig. 4 generated high thermal resistance during CO_2 adsorption and slow CO_2 adsorption. The other gases showed significant differences between the isosteric heats of adsorption but not between relative heat transfer rates. As a result, since the heat transfer rates were not sufficiently high to quickly release the produced heat, the order of adsorption rates on zeolite LiX followed the decreasing order of isosteric heat of adsorption.

4.3 Dependence of pressure and temperature on adsorption kinetics

Figure 5 represents the effective diffusion time constants of gases on zeolite LiX and activated carbon at 293 K as a function of pressure. The effective diffusion time constants for the gases were on the same order of magnitude except for that of the CO_2/zeolite LiX system. The effective diffusion time constants of some gases, especially N_2 on zeolite LiX and CO on activated carbon, increased slightly with pressure, while CO_2 and CO on zeolite LiX and CO_2 and CH_4 on activated carbon remained nearly constant. The pressure dependences may have arisen from changes in the slope of the adsorption isotherm and the isosteric heat of adsorption.

The diffusion in pelletized zeolites is affected by both micropore and macropore diffusions, but it is hard to determine the controlling diffusion mechanism of the zeolite system by the effective diffusion time constant. Thus, a controlling mechanism in zeolite pellet was indirectly examined by measuring the adsorption rate by changing the macropore diffusion length (Lee and Ruthven 1979). Figure 6 is the comparison between the effective diffusion time constants in different size pellets of zeolite LiX (1.5 and 0.8 mm). The effective diffusion time constant of CO_2 in Fig. 6a, that has the highest adsorption affinity to zeolite LiX, was not affected by the pellet size, whereas CO and CH_4 showed a little difference at a relatively low pressure range. It implied that the contribution of micropore diffusion to the effective diffusion time constants in CO_2, CO and CH_4/zeolite LiX systems is much higher than that of macropore diffusion.

The effective diffusion time constants of N_2 in zeolite LiX showed a certain difference between two different size pellets in Fig. 6b. The uptake at the smaller size pellet was

Table 2 Effective diffusion time constants and non-isothermal model parameters (ha/ρ_sC_s and β) of CO_2, CO, N_2 and CH_4 on zeolite LiX obtained from the experimental uptake curves and the non-isothermal model

CO_2						
293 K						
P (kPa)	19.9	30.6	44.4	52.4	61.3	80.7
D/R^2 (s^{-1})	7.71×10^{-3}	7.52×10^{-3}	7.84×10^{-3}	8.01×10^{-3}	8.14×10^{-3}	7.98×10^{-3}
ha/ρ_sC_s (s^{-1})	0.0125	0.0129	0.0141	0.0141	0.0150	0.0156
β (–)	0.220	0.294	0.441	0.467	0.586	0.693
308 K						
P (kPa)	22.7	35.4	42.7	59.2	68.4	77.9
D/R^2 (s^{-1})	1.06×10^{-2}	8.81×10^{-3}	1.17×10^{-3}	1.08×10^{-2}	9.77×10^{-3}	9.46×10^{-3}
ha/ρ_sC_s (s^{-1})	0.0142	0.0141	0.0142	0.0146	0.0154	0.0157
β (–)	0.203	0.221	0.380	0.445	0.579	0.628
323 K						
P (kPa)	25.2	47.4	56	65.1	74.5	84.3
D/R^2 (s^{-1})	1.38×10^{-2}	1.29×10^{-2}	1.32×10^{-2}	1.25×10^{-2}	1.12×10^{-2}	1.18×10^{-2}
ha/ρ_sC_s (s^{-1})	0.0157	0.0160	0.0161	0.0164	0.0178	0.0185
β (–)	0.232	0.328	0.397	0.421	0.566	0.605
CO						
293 K						
P (kPa)	23.3	32.8	43.2	54.2	65.7	77.7
D/R^2 (s^{-1})	3.02×10^{-2}	3.47×10^{-2}	3.51×10^{-2}	3.48×10^{-2}	3.41×10^{-2}	3.51×10^{-2}
ha/ρ_sC_s (s^{-1})	0.0242	0.0241	0.0283	0.0245	0.0290	0.0261
β (–)	0.208	0.250	0.371	0.343	0.506	0.439
308 K						
P (kPa)	21.2	30.3	40.4	51.5	63.1	75.1
D/R^2 (s^{-1})	2.94×10^{-2}	5.04×10^{-2}	4.37×10^{-2}	4.31×10^{-2}	5.05×10^{-2}	4.10×10^{-2}
ha/ρ_sC_s (s^{-1})	0.0251	0.0277	0.0273	0.0271	0.0272	0.0321
β (–)	0.213	0.268	0.290	0.322	0.347	0.536
323 K						
P (kPa)	19	28.3	38.7	50	62.1	74.1
D/R^2 (s^{-1})	2.76×10^{-2}	2.63×10^{-2}	4.96×10^{-2}	4.11×10^{-2}	5.19×10^{-2}	4.91×10^{-2}
ha/ρ_sC_s (s^{-1})	0.0231	0.0273	0.0286	0.0285	0.0301	0.0327
β (–)	0.155	0.232	0.276	0.332	0.360	0.493
N_2						
293 K						
P (kPa)	18.9	29.4	40.7	52.2	63.9	76.1
D/R^2 (s^{-1})	3.03×10^{-2}	3.93×10^{-2}	4.99×10^{-2}	5.33×10^{-2}	5.39×10^{-2}	5.43×10^{-2}
ha/ρ_sC_s (s^{-1})	0.0279	0.0287	0.0287	0.0327	0.0331	0.0326
β (–)	0.103	0.161	0.192	0.295	0.339	0.358
308 K						
P (kPa)	23.2	35.1	47.4	59.9	72.5	85.2
D/R^2 (s^{-1})	4.12×10^{-2}	5.04×10^{-2}	5.98×10^{-2}	6.83×10^{-2}	7.54×10^{-2}	7.24×10^{-2}
ha/ρ_sC_s (s^{-1})	0.0306	0.0290	0.0301	0.0356	0.0353	0.0359
β (–)	0.083	0.139	0.180	0.276	0.280	0.310
323 K						
P (kPa)	26.7	40	53.3	66.8	80.4	
D/R^2 (s^{-1})	5.03×10^{-2}	6.60×10^{-2}	7.20×10^{-2}	7.24×10^{-2}	7.17×10^{-2}	
ha/ρ_sC_s (s^{-1})	0.0287	0.0267	0.0304	0.0314	0.0366	
β (–)	0.0699	0.0989	0.157	0.213	0.299	

Table 2 continued

CH_4						
293 K						
P (kPa)	19	29	39.5	50.2	61.3	83.6
D/R^2 (s^{-1})	4.73×10^{-2}	6.31×10^{-2}	6.03×10^{-2}	6.94×10^{-2}	6.77×10^{-2}	6.41×10^{-2}
$ha/\rho_s C_s$ (s^{-1})	0.0300	0.0329	0.0341	0.0349	0.0379	0.0400
β (–)	0.081	0.124	0.177	0.226	0.295	0.375
308 K						
P (kPa)	22.6	33.9	45.6	57.2	69	80.4
D/R^2 (s^{-1})	6.01×10^{-2}	7.23×10^{-2}	7.03×10^{-2}	7.44×10^{-2}	6.33×10^{-2}	5.78×10^{-2}
$ha/\rho_s C_s$ (s^{-1})	0.0335	0.0323	0.0345	0.0353	0.0415	0.0453
β (–)	0.073	0.110	0.185	0.207	0.370	0.496
323 K						
P (kPa)	25.8	38.6	51.3	63.9	76.6	
D/R^2 (s^{-1})	7.38×10^{-2}	8.20×10^{-2}	8.21×10^{-2}	8.39×10^{-2}	6.87×10^{-2}	
$ha/\rho_s C_s$ (s^{-1})	0.0327	0.0333	0.0375	0.0369	0.0442	
β (–)	0.056	0.107	0.143	0.183	0.346	

faster in the whole pressure range. Therefore, the macropore diffusion worked as a controlling step in the effective diffusion time constant. However, the difference at a low pressure was relatively small when compared with the difference in N_2/zeolite 10X system (Ahn et al. 2002). It may stem from the relatively strong adsorption affinity of N_2 with zeolite LiX. Then, the difference between two different size pellets decreased with an increase in pressure, which could be interpreted as the transition of the controlling step from macropore diffusion to micropore diffusion. It was also confirmed that the effective diffusion time constants increased as the slope of isotherm decreased, which implied the decrease in macropore diffusion contribution with pressure (Hu et al. 2014; Ahn et al. 2002).

The diffusion rate in macropore controlled system is easily affected by pressure because the slope of isotherm decreases with pressure. If the slope of the isotherm is steep, adsorption potential is high near the adsorbent crystal surface when adsorbate molecules are trapped near the micropores, which resist diffusion in macropores (Ahn et al. 2004). As shown in Fig. 4a, the slopes of adsorption isotherms decreased with increasing pressure. In zeolite LiX, the slope changes of adsorption isotherms from pressures greater than 20 kPa became very small in CO_2 and CO, and those in N_2 and CH_4 were not significant over the entire pressure range. In activated carbon, the slope changes of adsorption isotherms were relatively smaller than those in zeolite LiX over the entire pressure range. The isosteric heats of adsorption in Fig. 4b decreased with increasing loading amount, resulting from decreasing adsorption affinities of CO_2 and CO with zeolite LiX and CO_2 and CH_4 with activated carbon. The other systems showed relatively constant heats of adsorption.

In Fig. 5, the adsorption rate increased because the influence of adsorption potential decreased with pressure. However, such phenomena were observed only in the low-pressure range, and the CO_2/adsorbent systems did not show any significant changes over the entire pressure range. Considering the slope change of the isotherms and the isosteric heat variation with pressure, the two phenomena had offsetting effects on adsorption rate. The CO/activated carbon system, which had relatively fast adsorption compared to the other systems, increased the effective diffusion time constant at high pressures. Because of the stepwise increment in pressure for the volumetric device, sufficiently high pressure guaranteed higher surface coverage on the adsorbent, which interrupted diffusion and adsorption of molecules on the adsorbent surface. The pressure effect on the adsorption rate is significant at low pressures and becomes weaker with increasing pressure.

The comparison of uptake curves between the two pressures is shown in Fig. 7. As mentioned before, adsorption was rapid in the early stages of all the systems and then approached equilibrium as the system became heat-controlled. At higher pressures, the uptake curve was smooth during the initial period of time, and the adsorption rate also was faster.

The uptake curves of the CO_2/zeolite system in Fig. 7a almost overlapped in the initial period time, and their difference gradually increased with time. The uptake curves of CO showed a similar trend. On the other hand, since the N_2/zeolite LiX system with slow heat transfer rates resulted in a heat-controlled system at higher pressures earlier than

Table 3 Effective diffusion time constants and non-isothermal model parameters (ha/ρ_sC_s and β) of CO_2, CO, N_2 and CH_4 on activated carbon obtained from the experimental uptake curves and the non-isothermal model

CO_2						
293 K						
P (kPa)	17.5	30.1	39.1	54.9	63.5	74.7
D/R^2	1.49×10^{-2}	2.23×10^{-2}	1.93×10^{-2}	1.73×10^{-2}	1.63×10^{-2}	1.54×10^{-2}
ha/ρ_sC_s (s^{-1})	0.0268	0.0244	0.0236	0.0231	0.0267	0.0240
β (–)	0.175	0.221	0.281	0.367	0.545	0.562
308 K						
P (kPa)	18.3	31.6	44.5	58.2	72.8	85.4
D/R^2	1.80×10^{-2}	2.01×10^{-2}	2.38×10^{-2}	1.84×10^{-2}	1.20×10^{-2}	1.27×10^{-2}
ha/ρ_sC_s (s^{-1})	0.0234	0.0248	0.0234	0.0261	0.0207	0.0210
β (–)	0.153	0.248	0.279	0.440	0.477	0.491
323 K						
P (kPa)	16.6	27.9	42.9	53.3	69.8	84.1
D/R^2	1.61×10^{-2}	1.93×10^{-2}	2.47×10^{-2}	2.17×10^{-2}	1.95×10^{-2}	2.10×10^{-2}
ha/ρ_sC_s (s^{-1})	0.0260	0.0249	0.0244	0.0244	0.0286	0.0272
β (–)	0.152	0.190	0.231	0.327	0.480	0.511
CO						
293 K						
P (kPa)	24.4	34	48.4	58	72	86.2
D/R^2	6.48×10^{-2}	7.62×10^{-2}	8.68×10^{-2}	8.87×10^{-2}	8.74×10^{-2}	9.19×10^{-2}
ha/ρ_sC_s (s^{-1})	0.0482	0.0457	0.0434	0.0441	0.0495	0.0470
β (–)	0.0856	0.119	0.139	0.186	0.276	0.266
308 K						
P (kPa)	26.6	37.3	47.5	57.6	72.5	87.2
D/R^2	8.30×10^{-2}	8.92×10^{-2}	9.38×10^{-2}	9.38×10^{-2}	1.01×10^{-1}	9.70×10^{-2}
ha/ρ_sC_s (s^{-1})	0.0470	0.0400	0.0455	0.0417	0.0480	0.0511
β (–)	0.0592	0.0868	0.123	0.150	0.177	0.254
323 K						
P (kPa)	22.9	34.1	45.1	55.7	71.5	86.8
D/R^2	7.67×10^{-2}	9.93×10^{-2}	1.00×10^{-1}	1.04×10^{-1}	1.20×10^{-1}	1.15×10^{-1}
ha/ρ_sC_s (s^{-1})	0.0328	0.0368	0.0427	0.0396	0.0428	0.0441
β (–)	0.0423	0.0518	0.0633	0.127	0.129	0.209
N_2						
293 K						
P (kPa)	18.8	32.5	46.2	55.4	69	82.7
D/R^2	4.42×10^{-2}	5.44×10^{-2}	6.45×10^{-2}	6.38×10^{-2}	5.68×10^{-2}	5.73×10^{-2}
ha/ρ_sC_s (s^{-1})	0.0120	0.0147	0.0158	0.0180	0.0194	0.0226
β (–)	0.144	0.183	0.206	0.250	0.321	0.572
308 K						
P (kPa)	20.8	31.1	41.2	56.2	70.7	89.6
D/R^2	5.96×10^{-2}	7.18×10^{-2}	7.76×10^{-2}	6.99×10^{-2}	7.30×10^{-2}	5.91×10^{-2}
ha/ρ_sC_s (s^{-1})	0.0150	0.0183	0.0174	0.0168	0.0215	0.0257
β (–)	0.145	0.201	0.243	0.269	0.355	0.736
323 K						
P (kPa)	22.4	33	43.7	54.2	69.6	84.9
D/R^2	7.45×10^{-2}	7.79×10^{-2}	7.49×10^{-2}	7.71×10^{-2}	8.04×10^{-2}	7.87×10^{-2}
ha/ρ_sC_s (s^{-1})	0.0138	0.0173	0.0182	0.0196	0.0206	0.0212
β (–)	0.182	0.237	0.296	0.365	0.466	0.463

Table 3 continued

CH_4						
293 K						
P (kPa)	22.4	34.4	46.8	59.3	71.9	84.7
D/R^2	6.10×10^{-2}	5.71×10^{-2}	5.29×10^{-2}	5.64×10^{-2}	5.87×10^{-2}	5.13×10^{-2}
ha/ρ_sC_s (s^{-1})	0.0622	0.0660	0.0696	0.0748	0.0792	0.0823
β (–)	0.140	0.268	0.364	0.524	0.606	0.753
308 K						
P (kPa)	25.6	38.4	51.3	64.6	77.8	
D/R^2	7.74×10^{-2}	7.16×10^{-2}	6.07×10^{-2}	5.90×10^{-2}	6.13×10^{-2}	
ha/ρ_sC_s (s^{-1})	0.0659	0.0633	0.0708	0.0799	0.0809	
β (–)	0.119	0.182	0.319	0.515	0.522	
323 K						
P (kPa)	28.4	42.3	56.1	69.7	83	
D/R^2	8.76×10^{-2}	8.19×10^{-2}	7.29×10^{-2}	5.59×10^{-2}	6.05×10^{-2}	
ha/ρ_sC_s (s^{-1})	0.0597	0.0583	0.0609	0.0656	0.0626	
β (–)	0.0802	0.146	0.186	0.429	0.391	

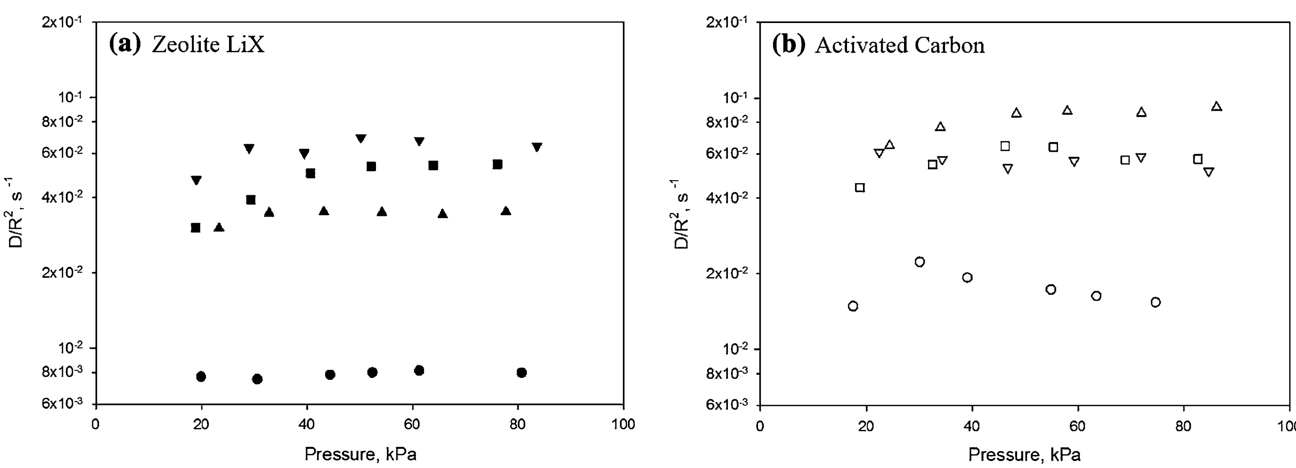

Fig. 5 Effective diffusion time constants (D/R^2) at 293 K obtained by non-isothermal diffusion model: **a** zeolite LiX and **b** activated carbon (*circle* CO_2; *up-pointing triangle* CO; *square* N_2; *down-pointing triangle* CH_4)

at lower pressures, the uptake curves showed a parallel decrease along the predicted lines by the heat controlled limit cases after passing certain period of time shown in Fig. 7b. CH_4 showed an uptake curve similar to that of N_2. As shown in Fig. 4b, the heats of adsorption of CO_2 and CO in zeolite LiX were relatively high and decreased with increasing loading amount, while those of N_2 and CH_4 were almost constant.

In the activated carbon systems, the uptake curves of CO_2 and CH_4 had the same trend as those of CO_2 and CO on zeolite LiX, while CO and N_2 showed similar behavior to N_2 and CH_4 on zeolite LiX during the initial period. As shown in Fig. 4b, the heats of adsorption of CO_2 and CH_4 were relatively high and decreased with an increasing loading amount, while those of CO and N_2 were almost constant. This implies that the initial uptake was strongly affected by the heat generated from adsorption.

Figure 8 represents the effect of temperature on the uptake curves of CO_2 as a representative case. The results at other pressure conditions are shown in Tables 2 and 3. The adsorption rate increased with temperature due to faster molecular diffusion with higher kinetic energy. The temperature dependence of the amount adsorbed was highest for N_2 on zeolite LiX and CH_4 on activated carbon (Park et al. 2014). The isotherm results according to temperature were in agreement with the dependence of the adsorption rates because lower surface coverage at higher temperature could result in an increased adsorption rate.

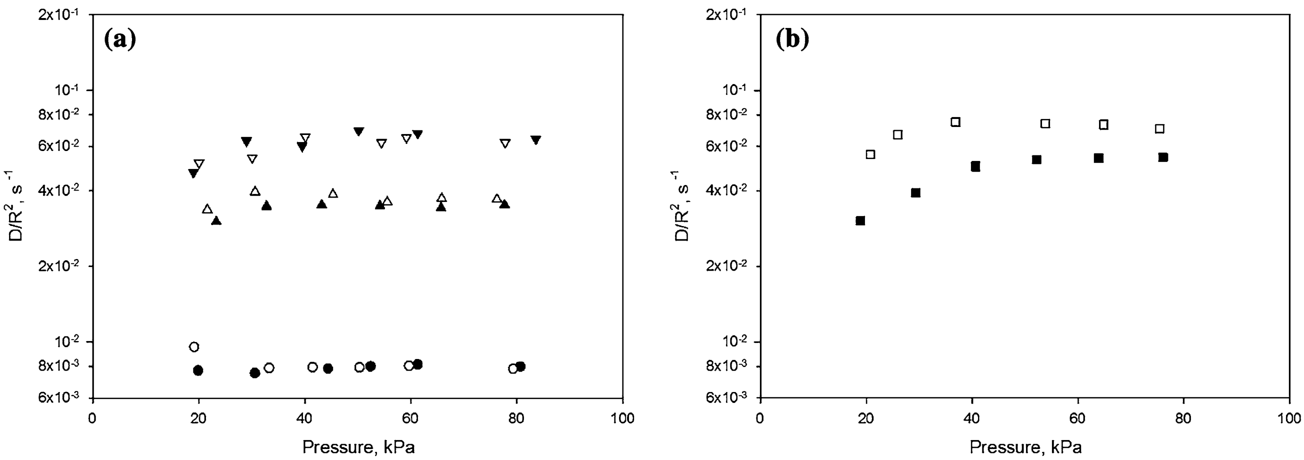

Fig. 6 Comparison of diffusion time constants for adsorption of **a** CO_2, CO, CH_4 and **b** N_2 in two different size of zeolite LiX pellet at 293 K: (*solid symbol* for 0.8 mm; *blank symbol* for 1.5 mm; *circle* CO_2; *up-pointing triangle* CO; *square* N_2; *down-pointing triangle* CH_4)

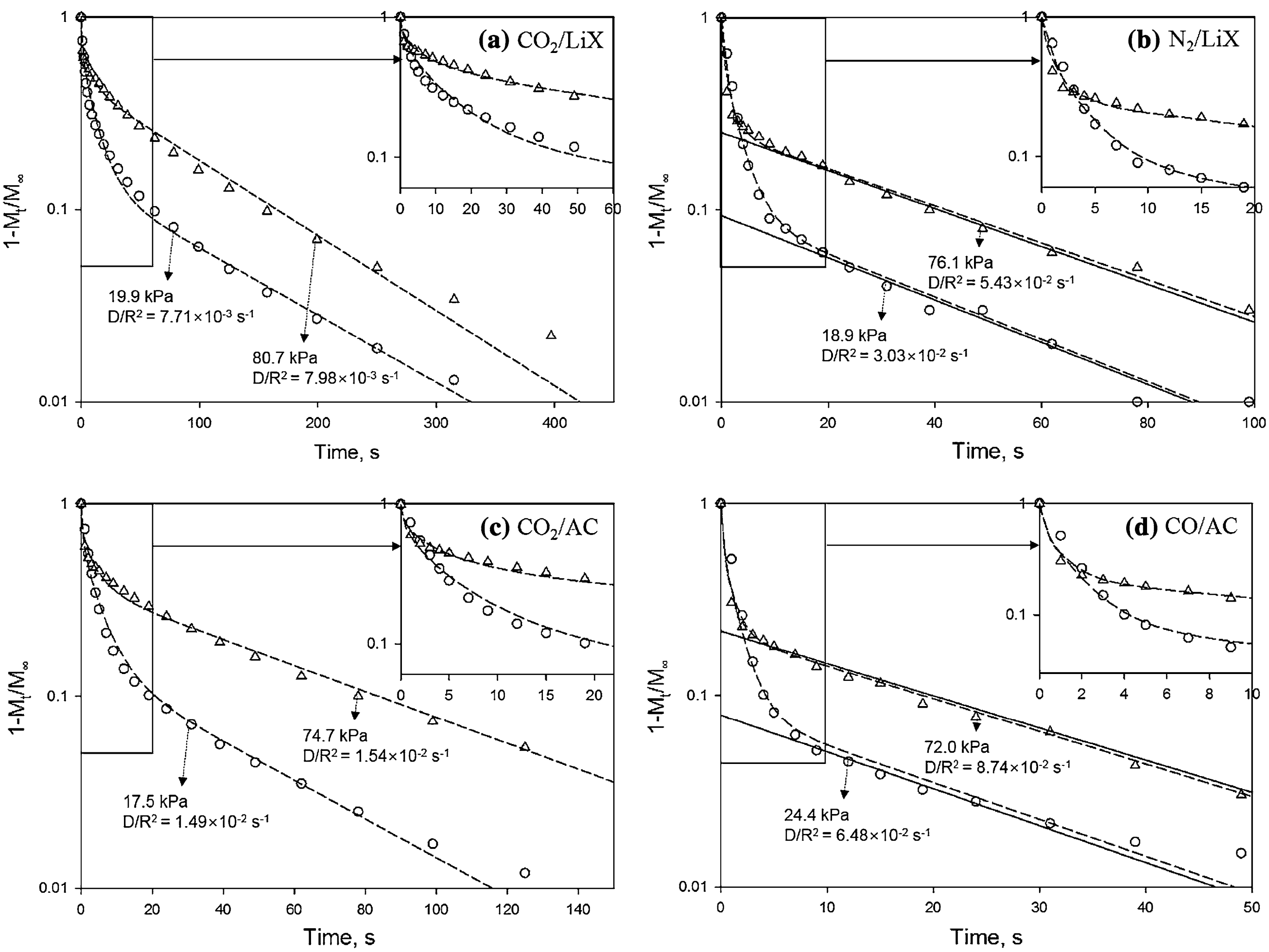

Fig. 7 Effect of pressure on uptake curves of **a** CO_2/zeolite LiX, **b** N_2/zeolite LiX, **c** CO_2/activated carbon, and **d** CO/activated carbon at 293 K. (*short dashed line* non-isothermal kinetic model; *solid line* heat transfer control limit)

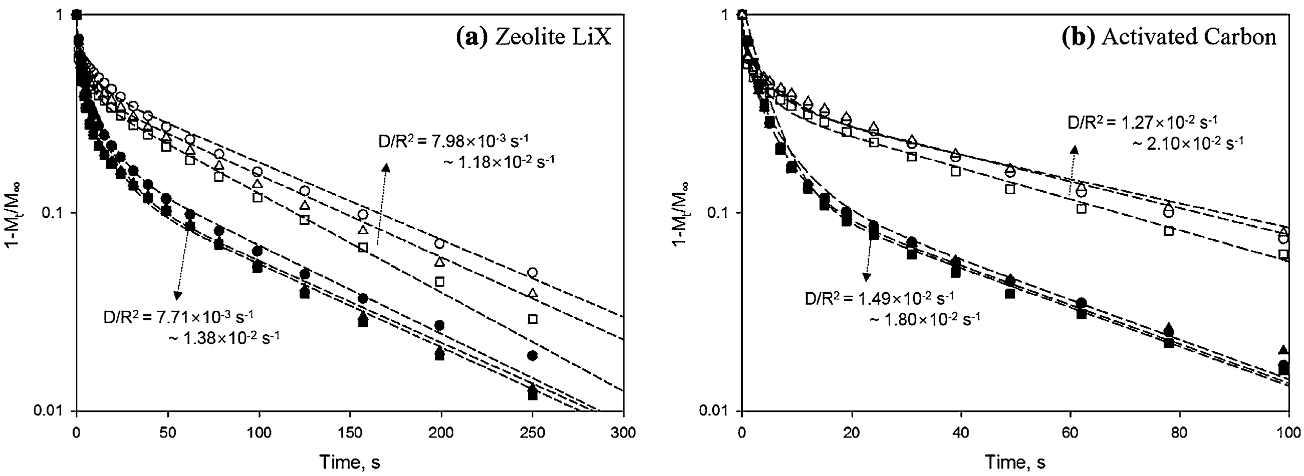

Fig. 8 Effect of temperature on uptake curves of CO_2: **a** zeolite LiX and **b** activated carbon (*circle* T = 293 K; *up-pointing triangle* T = 308 K; *square* T = 323 K; *solid symbol* for about 20 kPa; *blank symbol* for about 80 kPa; *short dashed line* non-isothermal diffusion model)

The level of temperature dependence depended on adsorbate/adsorbent system as well as applied pressure. Generally, the temperature effect on adsorption rate is stronger in a system with higher temperature dependence on equilibrium capacity. As shown in Fig. 8, the shapes of uptake curves of CO_2 at similar pressure were similar regardless of temperature and adsorbent. However, the effects of temperature on effective diffusion constant on zeolite LiX were similar regardless of pressure, while those on activated carbon were higher at higher pressure than at lower pressure.

5 Conclusion

The adsorption uptakes for CO_2, CO, N_2 and CH_4 on zeolite LiX and activated carbon were measured at 293, 308 and 323 K up to 100 kPa. The effective diffusion time constants (D/R^2) of each component on each adsorbent were obtained by fitting a non-isothermal kinetic model with experimental uptake curves.

At the same pressure and temperature, the order of adsorption rates on zeolite LiX was $CO_2 \ll CO < N_2 < CH_4$, but the isosteric heats of adsorption showed the opposite order ($CH_4 < N_2 < CO \ll CO_2$). The order of adsorption rates on activated carbon was arranged as $CO_2 \ll CH_4 \leq N_2 < CO$, but the sequence of adsorption rates was not perfectly matched with the order of isosteric heats of adsorption ($N_2 \leq CO < CH_4 < CO_2$).

The adsorption rates of the gases on zeolite LiX and activated carbon were affected by the isosteric heats of adsorption, heat transfer rate and adsorption affinity. Even though the heat of adsorption was small, it significantly affected the adsorption rate if the heat transfer rates were not sufficiently high to quickly release the generated heat. In addition, the initial uptake was strongly affected by the heat generated from adsorption.

The slope change in the isotherm and the isosteric heat variation with pressure produced an off-set effect on adsorption rate. The contribution of micropore diffusion on the zeolite LiX system seemed to be stronger than that of macropore diffusion. The effect of pressure on adsorption rate was significant at low pressure and became weaker with increasing pressure because of the decreased slope of the adsorption isotherm, decreased isosteric heat of adsorption and high surface coverage with pressure. The dependence of adsorption rate on temperature was in agreement with the isotherm results, showing that the adsorption rate increased with temperature.

Activated carbon granules and zeolite LiX pellets are widely used in adsorptive cyclic processes with respect to equilibrium separation for simple gas mixture. Even though adsorption equilibrium and selectivity work as a key factor in the separator design, the order of magnitude in the value of adsorption rate also contributes to improving the design accuracy in adsorptive separation processes. Therefore, the adsorption kinetic results obtained from the volumetric method in the study contribute to improving the design accuracy of various adsorptive processes using zeolite LiX and activated carbon for various effluent gases with CO_2, CO, N_2 and CH_4.

Acknowledgments We would like to acknowledge the financial support from the R&D Convergence Program of MSIP (Ministry of Science, ICT and Future Planning) and NST (National Research Council of Science & Technology) of Republic of Korea (CRC-14-1-KRICT).

References

Ahn, H., Moon, J.-H., Hyun, S.-H., Lee, C.-H.: Diffusion mechanism of carbon dioxide in zeolite 4A and CaX pellets. Adsorption **10**(2), 111–128 (2004)

Ahn, H., Yang, J., Lee, C.-H.: Effects of feed composition of coke oven gas on a layered bed H_2 PSA process. Adsorption **7**(4), 339–356 (2001)

Ahn, H., Yoo, H.-K., Shul, Y., Hyun, S., Lee, C.-H.: Diffusion mechanism of N_2 and CH_4 in pelletized zeolite 4A, 5A and CaX. J. Chem. Eng. Jpn. **35**(4), 334–345 (2002)

Ahn, S., You, Y.-W., Lee, D.-G., Kim, K.-H., Oh, M., Lee, C.-H.: Layered two-and four-bed PSA processes for H_2 recovery from coal gas. Chem. Eng. Sci. **68**(1), 413–423 (2012)

Bae, Y.-S., Lee, C.-H.: Sorption kinetics of eight gases on a carbon molecular sieve at elevated pressure. Carbon **43**(1), 95–107 (2005)

Cavenati, S., Grande, C.A., Rodrigues, A.E.: Separation of CH_4/CO_2/N_2 mixtures by layered pressure swing adsorption for upgrade of natural gas. Chem. Eng. Sci. **61**(12), 3893–3906 (2006)

Crank, J.: The Mathematics of Diffusion. Oxford University Press, London (1956)

Do, D.D.: Adsorption Analysis: Equilibria and Kinetics, vol. 2. Imperial College Press, London (1998)

Giesy, T.J., LeVan, M.D.: Mass transfer rates of oxygen, nitrogen, and argon in carbon molecular sieves determined by pressure-swing frequency response. Chem. Eng. Sci. **90**, 250–257 (2013)

Grande, C.A., Rodrigues, A.E.: Layered vacuum pressure-swing adsorption for biogas upgrading. Ind. Eng. Chem. Res. **46**(23), 7844–7848 (2007)

Gray, P.G., Do, D.D.: Dynamics of carbon dioxide sorption on activated-carbon particles. AIChE J. **37**(7), 1027–1034 (1991)

Himeno, S., Komatsu, T., Fujita, S.: High-pressure adsorption equilibria of methane and carbon dioxide on several activated carbons. J. Chem. Eng. Data **50**(2), 369–376 (2005)

Hu, X., Mangano, E., Friedrich, D., Ahn, H., Brandani, S.: Diffusion mechanism of CO_2 in 13X zeolite beads. Adsorption **20**(1), 121–135 (2014)

Kočiřík, M., Struve, P., Bülow, M.: Analytical solution of simultaneous mass and heat transfer in zeolite crystals under constant-volume/variable-pressure conditions. J. Chem. Soc. Faraday Trans. 1 **80**(8), 2167–2174 (1984)

Lee, H.-H., Lee, J.-C., Joo, Y.-J., Oh, M., Lee, C.-H.: Dynamic modeling of Shell entrained flow gasifier in an integrated gasification combined cycle process. Appl. Energy **131**, 425–440 (2014a)

Lee, J.C., Lee, H.H., Joo, Y.J., Lee, C.H., Oh, M.: Process simulation and thermodynamic analysis of an IGCC (integrated gasification combined cycle) plant with an entrained coal gasifier. Energy **64**, 58–68 (2014b)

Lee, J.J., Kim, M.K., Lee, D.G., Ahn, H., Kim, M.J., Lee, C.H.: Heat-exchange pressure swing adsorption process for hydrogen separation. AIChE J. **54**(8), 2054–2064 (2008)

Lee, L.-K., Ruthven, D.M.: Analysis of thermal effects in adsorption rate measurements. J. Chem. Soc. Faraday Trans. **1**(75), 2406–2422 (1979)

Linstrom, P., Mallard, W.: NIST Chemistry Webbook. NIST Standard Reference Database No. 69 (2001)

Park, Y., Moon, D.-K., Kim, Y.-H., Ahn, H., Lee, C.-H.: Adsorption isotherms of CO_2, CO, N_2, CH_4, Ar and H_2 on activated carbon and zeolite LiX up to 1.0 MPa. Adsorption **20**(4), 631–647 (2014)

Ruthven, D.M., Lee, L.K., Yucel, H.: Kinetics of non-isothermal sorption in molecular sieve crystals. AIChE J. **26**(1), 16–23 (1980)

Silva, J.A., Schumann, K., Rodrigues, A.E.: Sorption and kinetics of CO_2 and CH_4 in binderless beads of 13X zeolite. Microporous Mesoporous Mater. **158**, 219–228 (2012)

Siriwardane, R.V., Shen, M.-S., Fisher, E.P., Poston, J.A.: Adsorption of CO_2 on molecular sieves and activated carbon. Energy Fuels **15**(2), 279–284 (2001)

Yang, J., Lee, C.H.: Adsorption dynamics of a layered bed PSA for H_2 recovery from coke oven gas. AIChE J. **44**(6), 1325–1334 (1998)

Yang, Y., Ribeiro, A.M., Li, P., Yu, J.-G., Rodrigues, A.E.: Adsorption equilibrium and kinetics of methane and nitrogen on carbon molecular sieve. Ind. Eng. Chem. Res. **53**(43), 16840–16850 (2014)

You, Y.-W., Lee, D.-G., Yoon, K.-Y., Moon, D.-K., Kim, S.M., Lee, C.-H.: H_2 PSA purifier for CO removal from hydrogen mixtures. Int. J. Hydrogen Energy **37**(23), 18175–18186 (2012)